

Bounds on a singular attractor in Euler using vorticity moments

Robert M. Kerr

Department of Mathematics, University of Warwick, Coventry CV4 7AL, United Kingdom

A new rescaling of the vorticity moments and their growth terms is used to characterise the evolution of anti-parallel vortices governed by the 3D Euler equations. To suppress unphysical instabilities, the initial condition uses a balanced profile for the initial magnitude of vorticity along with a new algorithm for the initial vorticity direction. The new analysis uses a new adaptation to the Euler equations of a rescaling of the vorticity moments developed for Navier-Stokes analysis. All rescaled moments grow in time, with the lower-order moments bounding the higher-order moments from above, consistent with new results from several Navier-Stokes calculations. Furthermore, if, as an inviscid flow evolves, this ordering is assumed to hold, then a singular upper bound on the growth of these moments can be used to provide a prediction of power law growth to compare against. There is a significant period where the growth of the highest moments converges to these singular bounds, demonstrating a tie between the strongest nonlinear growth and how the rescaled vorticity moments are ordered. The logarithmic growth of all the moments are calculated directly and the estimated singular times for the different D_m converge to a common value for the simulation in the best domain.

PACS numbers:

To appear in the *Procedia IUTAM* volume of papers for Topological Fluid Dynamics II under
The growth of vorticity moments in the Euler equations

I. BACKGROUND

Two unresolved issues that have limited the application of numerics to the vortex dynamics and regularity questions of the three-dimensional Euler equations have been the inadequate analysis tools and the difficulties in specifying reproducible initial conditions. The existing analysis tools are unable to simultaneously cover the necessary range of scales in both space and time, while existing methods for mapping vortex tubes onto Eulerian meshes tend to generate ghost images unless *ad hoc* massaging is applied. This has led to weak and conflicting conclusions that depend upon the numerical method used and the choice of analysis that is applied to the results.

To address these problems, this paper introduces an improved initialization for curved vortex tubes following an arbitrary trajectory and new analysis that is based upon higher-order vorticity

moments, and then applies these to simulations of interacting anti-parallel vortices. The new initialisation suppresses core instabilities, which eliminates the ghost vortices found in earlier work [8] and discussed by [2]. Furthermore, the new trajectory algorithm allows the evolution of vortices with the same local perturbation, but different lengths, to be compared. One example calculation is given in Fig. 1. The new analysis allows one to compare all orders of the vorticity moments and generates new bounds against which to compare the results, which leads to more robust conclusions.

The new analysis tool is an adaptation to the inviscid Euler equations of a new rescaling of the vorticity moments for the viscous Navier-Stokes equations. The rescaling uses a new frequency ϖ_0 , plus scaling powers α_m , to convert the standard Ω_m , or L^{2m} , vorticity moments, into the following D_m moments [4, 5]:

$$D_m = (\varpi_0^{-1} \Omega_m)^{\alpha_m} \quad \text{where} \quad \Omega_m = \left(L^{-3} \int_V |\omega|^{2m} dV \right)^{1/2m}, \quad \varpi_0 = \varpi_\nu = \nu/L^2 \quad \text{and} \quad \alpha_m = 2m/(4m-3). \quad (1)$$

For the Navier-Stokes equations, ϖ_0 is based upon the viscosity ν and the characteristic large length scale L of the turbulence and the α_m are designed such that neighbouring $D_m(t)$ and $D_{m+1}(t)$ terms can be compared directly using Navier-Stokes vorticity moment inequalities. This is adapted to the inviscid case below. The new rescaling makes comparisons between all the moments of the vorticity possible, both analytically and numerically.

Historically, only the two limiting D_m have been used for addressing regularity questions. These are the global mean square vorticity or enstrophy, rescaled here into D_1 , and the point-wise maximum of vorticity $\|\omega\|_\infty$, rescaled into D_∞ . This is in part because analysis of the inequalities relating the intermediate moments had never been done. The known importance of D_1 is for addressing Navier-Stokes regularity (see references in [3]), while for the Euler equations, possible singularities are controlled by the time integral of $\|\omega\|_\infty$. That is, for the Euler equations, if

$$\int_0^t \|\omega\|_\infty d\tau < \infty \quad \text{for all time } t > 0, \quad (2)$$

then the Euler equations are regular [1]. authors]Beale, J.T.

The importance of the D_m between these limits is that by taking their ratios, new criteria for the regularity of the Navier-Stokes equations can be found [6]. To demonstrate the usefulness of the Navier-Stokes $D_m(t)$, Fig. 2(left) shows their evolution using data from a viscous, anti-parallel reconnection calculation using the initial condition described below. A full discussion of the trends, with lower order bounding higher order and convergence as m increases, is being prepared for publication.

To adapt this rescaling to vorticity moments of the inviscid Euler equations a non-viscous replacement for the scaling frequency ϖ_0 in (1) is needed. The inviscid modification chosen here defines ϖ_0 using the circulation of the vortices Γ instead of the viscosity ν . That is: $\varpi_0 = \varpi_\Gamma = \Gamma/L^2$.

For $m < \infty$, a computational advantage of using these inviscid D_m in numerical analysis of the Euler equations is that they and their time derivatives dD_m/dt can be determined at run-time and then compared as functions of time to integrals suggested by mathematical analysis. Furthermore, from the inverses of the logarithmic time derivatives $(d\log(D_m)/dt)^{-1} = D_m/(dD_m/dt)$, one can estimate the type of power-law singular growth using simple time differences [2] or, if it is assumed that the $D_m^{-2} \rightarrow a(T_m - t)$, running estimates of the $T_m(t)$ can be made without using time differences. These running estimates will be used in the final test for singular growth using data from the best of the new anti-parallel Euler calculations.

When these new Euler simulations were begun, the modest goal was to explain the type and strength of the convergence of the D_m moments in an early period of the Navier-Stokes calculation. The desired comparison period would be up to the beginning of the first vortex reconnection event at $t = 16$, shown in Fig. 1(right). Before $t = 16$, the viscous effects in the Navier-Stokes calculation should be negligible and the nonlinear terms, shared with the Euler equations, should dominate. The two frames in Fig. 2 are used to compare these D_m trends for the two Navier-Stokes and Euler calculations being highlighted here.

The observed ordering of the $D_m(t)$ for the Navier-Stokes simulations in Fig. 2(left), plus the period of extended singular growth of the D_m^{-2} Euler moments in Fig. 2(right) then led to Fig. 3. This figure addresses the question of whether the Euler equations have a singularity subject singularity using a new set of numerically determined time integrals and analysis of logarithmic time derivatives found at run-time. The new time integrals come from mathematical analysis of the Euler equations that assumes *a priori* that the order of the D_m seen numerically will hold for all time, as indicated by Fig. 2(right).

All the calculations are, fundamentally, in periodic computational domains, with symmetries used to decrease the data and time needed to do the calculations. Several filtered/dealiased pseudospectral methods have been tested and described previously [2]. The method chosen for the calculations here is a combination of the 2/3rds dealiasing rule plus a 36th order filtering method that was first introduced without dealiasing [8]. authors]Kerr, R.M. authors]Bustamante, M.D. authors]Hou, T.Y.

The principle axes are: x is the direction of propagation of the vortex pair, y is in the primary

direction of the vortices, and z is the direction between the vortices. The computed domain size is $L_x \times L_y \times L_z$, while the fully-periodic domain would be in $L_x \times 2L_y \times 2L_z$. Domain sizes and meshes are given in Table 1. Referring to the initial condition in Fig. 1, the $y = 0$ symmetry plane with the maximum perturbation will be called the *perturbation plane* and the $z = 0$ symmetry plane between the vortices will be called the *dividing plane*.

The paper is organised as follows. First, the new initial condition is described briefly. Next, the re-scaling of the vorticity moments for the Navier-Stokes and Euler equations is discussed further and applied to the new calculations, from which a new ordering for the $D_m(t)$ moments is found. This ordering has been found for all times for both the viscous and inviscid cases. After the new ordering is established, new upper bounds on the growth of the moments in the Euler equations are found and applied to the inviscid Euler solutions. Next, the logarithmic time derivatives of the D_m^2 from the Euler calculation are used to give running estimates of the singular times, labeled $T_m(t)$. It is found that for $m > 1$, these estimated times converge. That is, all the $T_m(t) \rightarrow T_c$. Finally, there is some discussion of additional diagnostics that are now being collected, such as the curvature of the vortex lines, that will be needed if we are going to understand why the Euler equations can obey singular scaling laws for extended periods.

II. INITIAL CONDITION

At meeting on the Euler equations in 2007 in Aussois, France, one topic was results from direct numerical simulations that addressed the question of regularity of the Euler equations. The conclusions of the two anti-parallel calculations [2, 7] were different, even though both were nominally using initial conditions similar to [11]. authors[Kerr, R.M. authors]Bustamante, M.D. authors[Hou, T.Y. Clearly, the prescription in [11] was flawed. These flaws have now been identified and will be described in detail in another paper. The three primary elements of the new initial condition are these:

- A new profile of the vorticity distribution in the core that is based upon the Rosenhead regularisation of a 2D point vortex and is similar to the two-dimensional density profiles used for quantum Gross-Pitaevskii calculations [13].
- A new direction algorithm that, for a given (x_i, y_j, z_k) on the three-dimensional grid, begins by finding the nearest position (x_s, y_s, z_s) on the given analytic trajectory. The distance used in the profile function for finding $|\omega|(x_i, y_j, z_k)$ is $r = |(x_i, y_j, z_k) - (x_s, y_s, z_s)|$ and

the direction of the vorticity at the points (x_i, y_j, z_k) is given by the tangent of the chosen trajectory at (x_s, y_s, z_s) .

- Making the vortices very, very long to minimise boundary effects.

The resulting profile has been used for anti-parallel vertical vortices in a stratified fluid, the anti-parallel unstratified Navier-Stokes calculations mentioned here, and now anti-parallel Euler vortices. In each case, unphysical initial instabilities due to small-scale imbalances have been suppressed, a cleaner and stronger larger-scale instability has been identified, and, where appropriate, a transition to sustained turbulence forms from the vortex interactions where none had been seen in earlier work. Unlike in earlier work [2, 11], no extra massaging or squeezing of the initial condition is needed to ensure that there is only one sign of the vorticity in the calculated $y = 0$ perturbation plane.

The computational procedure is as follows: First, the vortex is initialised on a modest mesh, which is then put onto a much larger computational mesh by adding zeros at the higher wavenumbers. The calculation then proceeds on this mesh until, by comparing results on different meshes, the collapse has progressed to the point where the calculation would soon be underresolved. Then the calculation is remeshed onto a finer mesh. Two remeshings are typically needed to reach the final mesh at the final times. The calculations used for the current study are given in the Table 1.

The initial and evolved Navier-Stokes vorticity isosurfaces in Fig. 1 apply to both the Navier-Stokes and Euler calculations because viscous dissipation for the Navier-Stokes case at $t = 16$ has been minimal. The insets show the upper/left quarter domain near the $y = 0$ perturbation plane, with the $t = 0$ inset showing that the initial vortex tube has a circular cross-section of constant width along its entire length.

These figures can be compared with similar stages in the evolution of anti-parallel quantum vortices in [13] and to the cover illustration in [12], which shows how the vortex lines twist as they extend from the $y = 0$ perturbation plane. The vortices do more than twist. They actually bend back upon themselves until, near $y = \pm 7$, they are closer than the unperturbed original vortices for $y > \pm 8$. The possible significance of this bend and its curvatur will be discussed in the summary.

III. NAVIER-STOKES INTERMITTENCY AND THE RESCALING VORTICITY MOMENTS

subject]vorticity moments

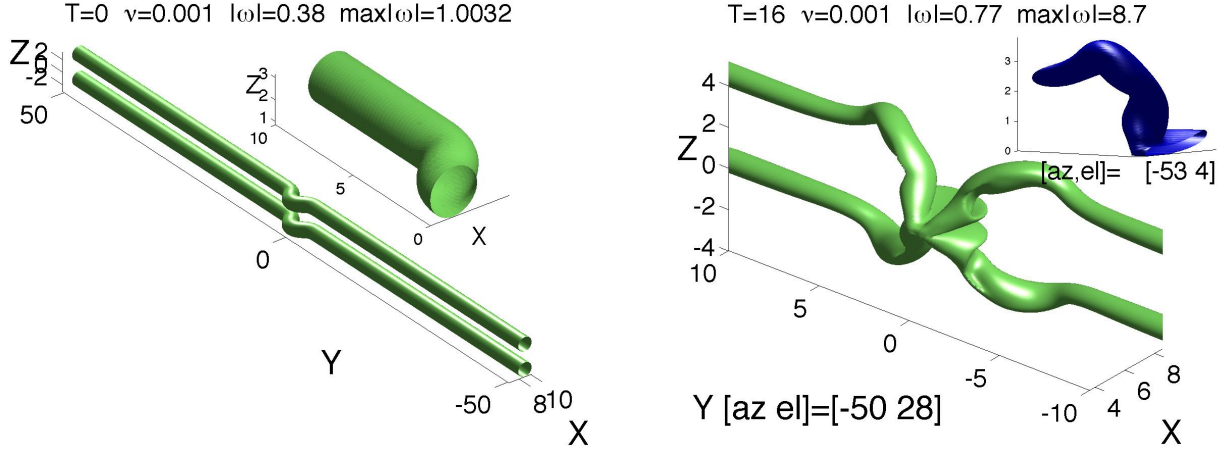


FIG. 1: **Left:** Very long, anti-parallel initial condition at $t = 0$. **Right:** $t = 16$ (Navier-Stokes). Insets show $z > 0$ for $0 \leq y \leq 10$.

A neglected topic in studying the Navier-Stokes equations is temporal intermittency, periods of intense activity, interspersed by relatively quiescent periods. One approach to characterising this type of intermittency is through higher-order strain ($[S] = S_{ij} = 0.5(\partial u_i / \partial x_j + \partial u_j / \partial x_i)$) and vorticity ($\omega = \nabla \times u$) moments, plus experimentally measurable single-point derivatives [17]. Numerically, convergent statistics for $\overline{S^{2m}}$ and $\overline{\omega^{2m}}$ with $m=2$ and 3 were obtained as early as 1985 [10].

However, having only orders $m=2$ and 3 is insufficient for making theoretical comparisons and it has been impossible to get convergent statistics for the next higher-order moments for even the largest forced simulations [9]. The problem is two-fold. First, the difference between the higher-moments moments in the quiet periods and the intense periods can be huge, and second, these occur on the time-scale of the large-scale forcing for simulations that, due to their size, can only be run for a few of these characteristic timescales.

Recently, Yeung, Donzis & Sreenivasan [18] authors]Yeung, P.K. have found that convergent statistics for their forced simulations can be obtained by taking ratios of the higher-order moments. While simultaneously, new mathematics has concluded that these ratios, rescaled in a manner consistent with inequalities for the time derivatives of the higher-order vorticity moments D_m [4], can give new insight into the Navier-Stokes singularity question [5], authors]Gibbon, J.D. as summarized in [14].

One analytic approach to answering whether the Navier-Stokes equations are regular or not starts by assuming that there are quiescent and intensely intermittent periods, called good and

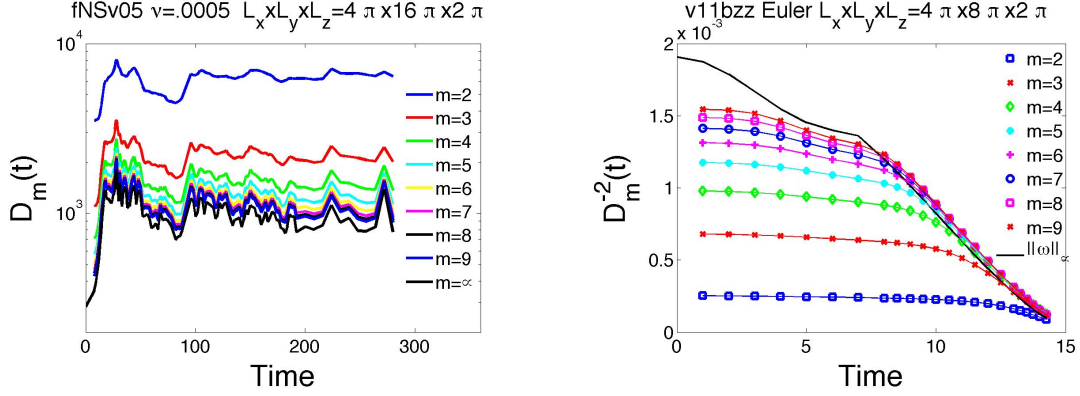


FIG. 2: **Left:** $Re = \Gamma/\nu = 4000$: D_m (1) from an anti-parallel calculation. D_m are ordered with lower-order bounding higher-order for all times. Especially note the the periods of steepest growth, $t < 16$ and $t \approx 90$ when the nonlinear terms dominate. **Right:** The inverses: $D_m^{-2}(t)$, from the Euler calculation with a similar initial condition for the first period of sharp growth ($t \leq 15$). The hierarchy of $D_m^{-2}(t)$ includes $\varpi/\|\omega\|_\infty$. The $D_m^{-2}(t)$ from the Navier-Stokes calculation are similar, but with a greater deviation from a linear form as time increases.

bad, or possibly neutral [4]. Because the $D_m(t)$ moments can be compared directly using vorticity moment inequalities, the new mathematics [5] is able to derive new bounds on the periods of the maximum growth of the D_m that can be compared to numerical results.

Fig. 2(left) shows how the D_m are ordered for the new reconnection calculation, with the lower order D_m bounding the higher order D_m for all times: $D_{m+1}(t) < D_m(t)$. This means that the different D_m never cross one-another and the definitions of bad and good periods are the same for all of the D_m . This ordering of lower-order above higher-order D_m was unexpected because it is opposite of how the original Ω_m , without rescaling, are required to be ordered using Hölder inequalities and is opposite to what would easily ensure regularity of the Navier-Stokes equations using the new bounds of [5]. authors]Gibbon, J.D. This ordering has now been identified in every Navier-Stokes simulation it has been tested against. A joint paper is in preparation and mentioned in [6].

What governs the dynamics during these intense/bad and quiet/good periods? Fig. 1(right) shows the structures at the end of the most extreme growth of the $D_m(t)$, up to $t = 16$, when the first Navier-Stokes vortex reconnection is forming. In a new Navier-Stokes reconnection paper it will be shown that all of the subsequent periods of intense growth of the higher-order D_m can be tied to how vortices are attracted and stretched just before reconnection events.

IV. RESCALED VORTICITY MOMENTS AND THE EULER EQUATIONS

The strongest growth of the Navier-Stokes D_m in Fig. 2(left) is before the first reconnection at $t \approx 16$, when viscous effects are negligible and the nonlinear Euler dynamics are strongest. During this period, the growth of the normalised enstrophy production, a skewness factor, is up to three times the values typically determined in large Reynolds number experiments and simulations. In order to understand the origins of this period of growth, a new series of simulations of the Euler equations were begun that cover part of this period ($t \leq 14.25$). The particular calculation shown is just one of a series of new anti-parallel inviscid Euler calculations outlined in Table 1, all using the new profile and trajectory algorithms. The objective was to find, and confirm, whether a domain could be identified where the boundaries were not suppressing any growth of the maximum of vorticity $\|\omega\|_\infty$. And then, determine if this calculation indicates singular behaviour, or not.

It was found that changing the length of the domain in the y -direction had the greatest effect upon the growth of $\|\omega\|_\infty$, with its growth being suppressed until $L_y = 8\pi$ was reached, the case labeled v11bzz. The v11g case with $L_y = 16\pi$ gave identical results to the v11bzz case.

The choice of $\varpi_0 = \varpi_\Gamma$ for the Euler D_m analysis was in part inspired by how the growth of enstrophy in an earlier Euler calculation [15] could be explained empirically by replacing viscosity ν with the circulation Γ in the well-known inequality for the upper bound on enstrophy growth in Navier-Stokes: $(d/dt)\Omega_1^2 \leq C_1(\Omega_1^2/(\nu/L^2))^3$. This empirical guess can now be replaced by robust Euler bounds that use the D_m with $\varpi_0 = \varpi_\Gamma$.

Following the proof of Proposition 1 [6], one starts with:

$$2mL^3\Omega_m^{2m-1}\frac{d}{dt}\Omega_m \leq 2mL^3c_{1,m}\Omega_{m+1}^{m+1}\Omega_m^m \quad (3)$$

which, with some rearranging, becomes

$$\frac{d}{dt}\Omega_m \leq c_{1m}, \left(\frac{\Omega_{m+1}}{\Omega_m}\right)^{m+1} \Omega_m^2. \quad (4)$$

Finally, upon substituting the definition of the D_m and pulling the ϖ_0 out, one gets

$$\frac{d}{dt}D_m \leq c_{2,m}\varpi_0 \left(\frac{D_{m+1}}{D_m}\right)^{\xi_m} D_m^3 \quad \text{where} \quad \xi_m = \frac{1}{2}(4m+1). \quad (5)$$

Once $\varpi_0 = \varpi_\Gamma$ is chosen, then the inviscid $D_m(t)$ can be compared for the Euler calculation. This has been done in same manner as in Fig. 2(left) and shows the same ordering as in the Navier-Stokes case[19]. However, in order to include the $m \rightarrow \infty$ limit, a better choice is to plot $D_m^{-2}(t)$, which for $m = \infty$ gives $D_\infty^{-2} = \varpi_\Gamma/\|\omega\|_\infty$, where $\|\omega\|_\infty$ is the $\sup(|\omega|)$. A simple test for

singular behaviour is to compare $1/\|\omega\|_\infty$ against the power law consistent with the lower bound for singular growth of $\|\omega\|_\infty$ allowed by (2). That is:

$$\|\omega\|_\infty \sim (T_\infty - t)^{-1} \quad \text{or} \quad D_\infty^{-2} = \varpi_\Gamma / \|\omega\|_\infty \sim \varpi_\Gamma (T_\infty - t). \quad (6)$$

Under this test, the sign of singularity growth would be finding that $D_\infty^{-2} \rightarrow 0$ linearly.

The $D_m^{-2}(t)$ are plotted in Fig. 2(right). Compared in this way, as m becomes large, the D_m nearly match $\varpi_\Gamma(T_\infty - t)$ as t increases. However, the growth of $\|\omega\|_\infty$ appears to tail off of this behaviour as $t \rightarrow 15$. So, to claim singular growth, another independently calculated diagnostic is needed to confirm the trends seen in Fig. 2(right).

If the only diagnostic for singular growth is $\|\omega\|_\infty$, then an appropriate secondary diagnostic could be $\alpha = d \log \|\omega\|_\infty / dt$, the logarithmic time derivative of $\|\omega\|_\infty$. In principle one should determine α from the vortex stretching exactly at the position of $\|\omega\|_\infty$. However, to get the stretching at the exact position of $\|\omega\|_\infty$, which lies between the mesh-points in physical space, requires interpolation, which can be both difficult and inaccurate. In practice, the only stretching diagnostic that did not have grid-induced oscillations and was near, but not at, the position of $\|\omega\|_\infty$, was to take the maximum of the vortex stretching on the perturbation plane [11].

Using the D_m resolves this problem. The trick is to calculate both the D_m and their time derivatives $(d/dt)D_m$ at run-time, a simple matter of programming compared to the interpolations needed for determining α at $\|\omega\|_\infty$. Furthermore, Fig. 2(right) shows that as time and m increase, the $D_m^{-2}(t) \rightarrow D_\infty^{-2}(t) = \varpi_\Gamma / \|\omega\|_\infty$. Therefore, for large m , the secondary diagnostics equivalent to α are the logarithmic time derivatives of the $D_m(t)$, which are used below to define the estimated singular times $T_m(t)$

Numerical analysis using new Euler integrals

With the added assumption that the D_{m+1}/D_m are always bounded, as demonstrated by Fig. 2(right), let us use the bound in (5) to help us write new Euler bounds that can be tested numerically.

For general m , let us begin by rewriting (5) as

$$-\frac{d}{dt}D_m^{-2} \leq c_m \varpi_\Gamma \left(\frac{D_{m+1}}{D_m} \right)^{\xi_m}, \quad \text{then using} \quad F_m(t) = c_m \int_0^t \varpi_\Gamma \left(\frac{D_{m+1}}{D_m} \right)^{\xi_m} dt \quad \text{one gets} \quad D_m^{-2} \leq c_{2,m} F_m(t). \quad (7)$$

This focuses our attention upon the integrals on the right-hand-side, which are plotted in Fig. 3(left). In this figure, the upper bound, based upon the integral of D_m^{-2} , grows linearly. If obeyed

exactly, this would imply that the solutions are singular. However, since this is only an upper bound, another test is needed.

This final test will be a diagnostic coming from the logarithmic time derivatives of the D_m^2 . Two assumptions are made. First, that $D_m^2(t) \sim (T_m - t)^{-\gamma_m}$ and second an assumption on the γ_m . Applying $(d \log D_m^2/dt)^{-1}$ to the first assumption, one gets

$$(d \log D_m^2/dt)^{-1} = \gamma_m^{-1}(T_m - t). \quad (8)$$

By applying this assumption to time differences of the $(d \log D_m^2/dt)^{-1}$, one could get running estimates of both the γ_m and the T_m . However, since as m increases the curves generated by the $D_m^2(t)$ are becoming linear in both Fig. 2(right) and Fig. 3(left), that is $\gamma_m \rightarrow 1$, the best way to find running estimates of the $T_m(t)$ is to make $\gamma_m \equiv 1$ an added assumption and use

$$T_m(t) = (d \log D_m^2/dt)^{-1} + t. \quad (9)$$

The result is in Fig. 3(right). For $t \gtrsim 12$, the estimated $m \geq 3$ singular times $T_m(t)$ are beginning to converge. This is shown more clearly by adding a $t = t$ curve and extending the computed T_m with linear extensions based on the T_m at the last two times computed. If there is a singularity of the Euler equations for this initial condition, then they should all cross the $t = t$ line at the same time. Which they do.

TABLE I: Domains and sequences of meshes used to resolve.

Domain	label	Mesh 1 and Mesh 3	Δt	Mesh 2 and Mesh 4	Δt
$3\pi \times 3\pi \times 2\pi$	v11a	$512 \times 256 \times 512$	$t = 0 - 12$	$512 \times 256 \times 1024$	$t = 8 - 15$
$3\pi \times 3\pi \times 2\pi$	v11a	$1024 \times 512 \times 4096$	$t = 10 - 13.25$	$1024 \times 512 \times 2048$	$t = 4 - 15$
$4\pi \times 4\pi \times 2\pi$	v71	$512 \times 512 \times 1024$	$t = 0 - 12$	$1024 \times 512 \times 2048$	$t = 12 - 13.5$
$4\pi \times 4\pi \times 2\pi$	v71	$1024 \times 512 \times 4096$	$t = 13.5 - 14.25$		
$4\pi \times 6\pi \times 4\pi$	v11by	$512 \times 256 \times 2048$	$t = 0 - 12$	$1024 \times 512 \times 2048$	$t = 8 - 14$
$4\pi \times 4\pi \times 4\pi$	v11bx	$1024 \times 512 \times 2048$	$t = 0 - 14$	$1024 \times 512 \times 4096$	$t = 11 - 14.25$
$4\pi \times 8\pi \times 4\pi$	v11bz	$512 \times 512 \times 1024$	$t = 0 - 12$	$1024 \times 1024 \times 4096$	$t = 12 - 13.75$
$4\pi \times 8\pi \times 2\pi$	v11bzz	$512 \times 512 \times 1024$	$t = 0 - 12$	$1024 \times 512 \times 2048$	$t = 12 - 13.5$
$4\pi \times 8\pi \times 2\pi$	v11bzz	$1024 \times 512 \times 4096$	$t = 13.5 - 14.25$		
$4\pi \times 16\pi \times 2\pi$	v11g	$512 \times 1024 \times 1024$	$t = 0 - 12$	$512 \times 1024 \times 2048$	$t = 12 - 14.25$
$4\pi \times 16\pi \times 2\pi$	v11g	$1024 \times 2048 \times 2048$	$t = 10 - 14$	$1024 \times 2048 \times 4096$	$t = 13 - 14.5$

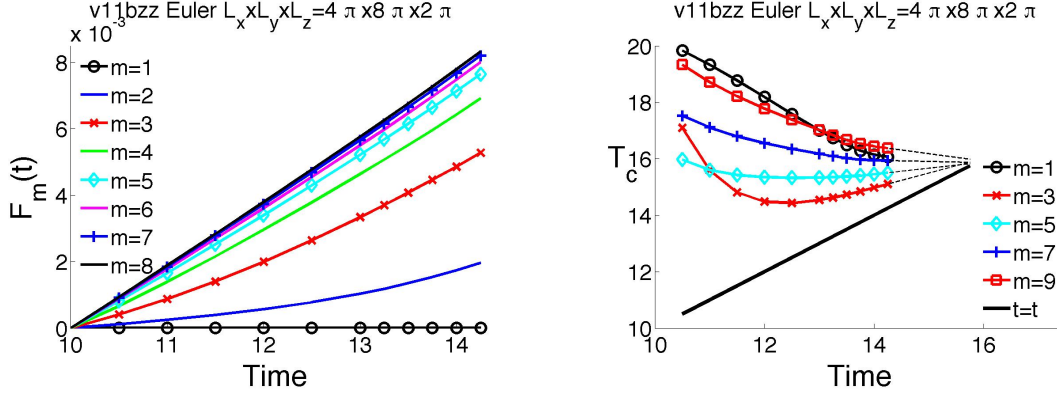


FIG. 3: **Left:** $\int \varpi_{\Gamma}(D_{m+1}/D_m)^{\xi_m} dt$ (7) for an anti-parallel Euler calculation. The observed ordering and linear increase as $m \rightarrow \infty$ would permit at least super-exponential growth of the D_m for both Euler and Navier-Stokes up to $t = 14.5$. **Right:** Estimated singular time from different D_m : $T_m(t) = (d \log D_m^2/dt)^{-1} + t$. Only m odd are shown to reduce clutter and a curve with $t = t$ is added to clarify where the $T_m(t)$ are heading. Linear extrapolations to $t = 15.75$ of the $m > 1$ curves, based on the last two values, are shown with the dashed lines. As well as could be expected, these extrapolations all appear to be crossing the $t = t$ line at about $T_c \approx 15.8$. For $t > 12$ (and excluding $m = 1$), the $T_m(t)$ are ordered. Going from underestimating the T_c ($m = 3, 5$) to overestimating T_c ($m = 7, 9$).

V. SUMMARY

A new approach to rescaling vorticity moments, the D_m , has been used for the analysis of new Navier-Stokes and Euler calculations. The D_m have the following favourable analytic and numerical properties: In mathematical analysis, neighbouring orders can be compared using their time derivatives inequalities [6]. In numerical analysis, their values, time derivatives and thus their logarithmic times derivatives can be determined continuously and compared.

The numerical comparisons have revealed an unexpected hierarchy where the lower-order D_m bound the higher-order D_m , for all times and for both sets of calculations. This ordering of the D_m was unexpected for two reasons. First, it is opposite to the required Hölder ordering of the Ω_m and second, it is opposite to an ordering that would immediately imply that the Navier-Stokes equations are regular for all times.

Furthermore, the period of strongest growth and alignment of the $D_m(t)$ occurs when the normalized enstrophy growth for the Navier-Stokes calculations is strongest. These observations led to the secondary goal of the Euler calculations. This is to use the D_m , and their logarithmic growth rates, to determine whether these Euler calculations are consistent with the formation a

finite-time singularity.

The new Euler calculations are consistent with the formation a finite-time singularity in the sense that each of the higher-order moments in Fig. 2 show singular trends for a longer period than any previous Euler calculation. This includes D_∞^2 , the rescaled singular maximum of the vorticity $\|\omega\|_\infty$. Critical to achieving this extended period of singular Euler growth is using vortices that are not subject to internal instabilities and domains that are longer than in any earlier work. However, using the new profile and direction algorithm is not enough. For the smaller domains listed in Table 1, the singular growth saturates early, as in some earlier work [8]. The importance of the longer domain is that it allows the full effect of the curvature and torsion of the vortices to manifest itself. It was not until the length of the domains was $L_y = 8\pi$ that the extended period of singular growth appeared.

With the new data set and new results, a number of outstanding questions will soon be addressed. One is determining the role of the curvature of the vortex lines. New analysis shows that the curvature of the vortex lines near $\|\omega\|_\infty$ is small, and therefore contributes little to the local $y = 0$ vortex stretching. This suggests that the stretching is coming from the strong curvature and looping seen in Fig. 1 (right) at $t = 16$ for $y = \pm 5$. Even though this structure is forming far from the position of $\|\omega\|_\infty$ on the $y = 0$ perturbation plane, its effects upon the growth on that plane are surprisingly strong.

This success with finding the curvature suggests that are further conditions on properties derived from the direction of the vorticity can be determined and tested against the growth of $\|\omega\|_\infty$. The new data should be capable of testing these proposed constraints and identifying how the position of the maximum of vorticity moves with respect to the Lagrangian flow. This relative motion is non-zero [?] and could be important for determining how the circulation in the perturbation plane becomes divided into a head and flattened tail, where the head is the part of the circulation that reconnects if there is viscosity.

-
- [1] Beale JT, Kato T, Majda A. Remarks on the breakdown of smooth solutions of the 3-D Euler equations *Commun. Math. Phys.* 1984;94:61.
 - [2] Bustamante MD, Kerr RM. 3D Euler about a 2D symmetry plane *Physica D* 2008;237:1912–1920.
 - [3] Doering CR. The 3D Navier-Stokes Problem *Ann. Rev. Fluid. Mech.* 2009;41:109128.
 - [4] Gibbon JD. Regularity and singularity in solutions of the three-dimensional NavierStokes equations *Proc. R. Soc. A* 2010;466:2587–2604.

- [5] Gibbon JD. Conditional regularity of solutions of the 3D Navier-Stokes equations & implications for intermittency *J. Math. Phys.* 2012;53:115608.
- [6] Gibbon JD. Dynamics of scaled norms of vorticity for the three-dimensional Navier-Stokes and Euler equations. *Topological Fluid Dynamics II* 2012;This volume.
- [7] Hou TY. Blow-up or no blow-up? The interplay between theory and numerics. *Physica D* 2008;237:1937–1944.
- [8] Hou TY, Li R. Dynamic depletion of vortex stretching and non-blowup of the 3-D incompressible Euler equations. *J. Nonlin. Sci.* 2006;16:639–664.
- [9] Ishihara T., Gotoh T., Kaneda Y.. Study of high-Reynolds number isotropic turbulence by direct numerical simulation *Annu. Rev. Fluid Mech.* 2009;41:16–180.
- [10] Kerr RM. Higher-order derivative correlations and the alignment of small-scale structures in isotropic numerical turbulence. *J. Fluid Mech.* 1985;153:31.
- [11] Kerr RM. Evidence for a singularity of the three-dimensional, incompressible Euler equations *Phys. Fluids A* 1993;5:1725–1746.
- [12] Kerr RM. Cover illustration: vortex structure of Euler collapse. *Nonlinearity* 1996;9:271–272.
- [13] Kerr RM. Vortex stretching as a mechanism for quantum kinetic energy decay *Phys. Rev. Lett.* 2011;106:224501.
- [14] Kerr RM. . *J. Fluid Mech.* 2012;700:1–4.
- [15] Kerr RM, Bustamante MD. Exploring symmetry plane conditions in numerical Euler solutions In: J.C Robinson, J. Rodrigo, W. Sadowski, editors. *Proceedings of Workshop on Partial Differential Equations and Fluid Mechanics*. University of Warwick, July 2010. Cambridge University Press 2011 .
- [16] Kerr RM, Hussain F. Simulation of vortex reconnection *Physica D* 1989;37:474-484.
- [17] Sreenivasan K.R., Antonia R.A.. The phenomenology of small-scale turbulence *Annu. Rev. Fluid Mech.* 1997;29:435–472.
- [18] Yeung PK, Donzis DA, Sreenivasan KR. Dissipation, enstrophy and pressure statistics in turbulence simulations at high Reynolds numbers *J. Fluid Mech.* 2012;700:5–15.
- [19] Note that if the rather low frequency of $\varpi_\Gamma = \Gamma/L^2$ is replaced by the much larger initial maximum of vorticity $\|\omega(t=0)\|_\infty$, this clean ordering is not found.